Int. J. Electrochem. Sci., 12 **(2017)** 9798 – 9811, doi: 10.20964/2017.10.89

International Journal of
ELECTROCHEMICAL
SCIENCE
www.electrochemsci.org

Preparation of a Natural Rubber Nanocomposite Coating based on Fe_3O_4@Carbon materials and their Corrosion Resistance

Yan Wang[1], *Yaya Zhou*[1], *YiBin Ma*[1], *Hongbin Lu*[2], *Youyi Sun*[1,2,*], *GuiZhe Zhao*[1], *Yaqing Liu*[1,2,*]

[1] Shanxi Province Key Laboratory of Functional Nanocomposites, North University of China, Taiyuan 030051, China;
[2] State Key Laboratory of Molecular Engineering of Polymer, Fudan University, Shanghai 200433, China
[*]E-mail: syyi@pku.edu.cn, lyqzgz2010@163.com

Received: 27 April 2017 / *Accepted:* 3 July 2017 / *Published:* 12 September 2017

Fe_3O_4@carbon nanomaterials/natural rubber (NR) nanocomposite coatings were prepared via a latex compounding method, in which the carbon nanomaterials (e.g., reduced graphene oxide (rGO), graphene oxide (GO) and carbon nanotubes (CNTs) were efficiently dispersed in NR latex with the aid of Fe_3O_4 nanoparticles. Furthermore, the barrier properties of the various Fe_3O_4@carbon nanomaterials/NR nanocomposite coatings were studied and compared via electrochemical impedance spectroscopy, optical microscopy and potentiodynamic polarization. These results revealed that the Fe_3O_4@CNT/natural rubber nanocomposite coating was a better barrier against corrosive media compared with Fe_3O_4@GO or Fe_3O_4@rGO doped natural rubber coatings. Moreover, the Fe_3O_4@CNT/natural rubber nanocomposite coating maintained its high anticorrosive properties with a low Rrcco (ca. 5.2×10^{-4} mm/year) and Icorr (0.05 μA/cm^2) over 10 cyclic bends (ca. 120^o). Enhanced flexible anticorrosion performance was observed because the Fe_3O_4 growing on the carbon nanomaterials surface avoided carbon materials/metal connections, thus increasing the electrical resistance of the coating. Additionally, the as-prepared composite coatings were flexible and their structures were less disordered, which could greatly prolong the diffusion pathway of corrosive media in the coating matrix.

Keywords: Carbon nanomaterials; natural rubber latex; nanocomposites; latex compounding; anticorrosive properties.

1. INTRODUCTION

Recently, carbon nanomaterials (e.g., graphene, graphene oxide and CNT) have been reported to be outstanding corrosion protection materials because they possess many unique properties which

are beneficial for anticorrosion, such as chemical stability, chemical inertness, remarkable flexibility, excellent thermal, and impermeability to molecules [1-2]. In addition to this, polymeric coatings have attracted considerable interest because they are lightweight, low-cost and can be fabricated inexpensively and easily by cost-effective techniques, e.g., inkjet, spray coating [3]. Therefore, the use of carbon nanomaterials (e.g. graphene, graphene oxide and CNT)-reinforced polymer composite coatings in anticorrosion applications have been reported because these coatings possess passive properties derived from the coating matrix (e.g., barrier, color, and adhesion), and improved physical properties (e.g., better mechanical performance, higher thermal and dimensional stability, and good barrier properties) [1-12]. For example, Chang et al. [4] described the first application of polymer/graphene composites for the anticorrosion of steel. The steel was able to be protected by the coating because of its impermeability to O_2 and H_2O. Yu et al. [5] successfully obtained well-dispersed PS/modified-GO composites via in situ mini-emulsion polymerization and the products were used for corrosion protection. Compared with pure polystyrene, the as-prepared composites presented superior anticorrosion properties. Zhang et al. [6] prepared an outstanding epoxy/graphene composites anticorrosive coating. Despite the strong interest in the scientific literature on the use of carbon nanomaterials (e.g., GO, rGO and CNT) for reinforced polymer hybrid coatings for protection and chemical insulation of metal substrates, most of the investigations have focused on a plastic matrix, which is less flexible. In this respect, the plastic coatings were difficult to apply for the corrosion prevention of flexible metal films and pipes. Therefore, it is critical and necessary to develop a flexible corrosion barrier for various applications.

In fact, carbon nanomaterials (e.g., GO, rGO or CNT)reinforced NR polymeric substances have been used in aggressive environments, especially in industry, due to their high durability, easy formability, flexibility, good chemical resistance and weather-resistance characteristics [13-15]. Therefore, it is vital to evaluate the anticorrosion performance of carbon materials (e.g., GO, rGO or CNT) reinforced NR nanocomposite coatings, applied as flexible corrosion barriers. However, to our knowledge, there has not been an investigation on the anticorrosion properties of different NR nanocomposite coatings containing either GO, rGO or CNT. In addition, there is a need to address the existing challenges and problems in the field of NR nanocomposites containing GO, rGO or CNT as flexible anticorrosion coatings, such as how to maintain good dispersion in NR latex for rGO or CNT an how to vulcanize the NR coating at low temperatures.

The purpose of this paper was to develop a flexible anticorrosion coating based on carbon nanomaterials and natural rubber latex. In this case, the incorporation of Fe_3O_4@GO, Fe_3O_4@CNT and Fe_3O_4@rGO was facilitated by interacting with the NR-latex matrix in an attempt to improve the dispersion and anticorrosion properties of the nanocomposite coatings. Significantly, the effects of the various carbon nanomaterials (GO, CNT and rGO) on the anticorrosion properties of the NR coating were investigated in detail. Furthermore, this work provided additional insight into the requirements of the Fe_3O_4 surfactant used to incorporate GO, CNT and rGO into the NR-latex matrix and opensthe possibility for the development of frontier and multifunctional materials.

2. EXPERIMENTAL SECTION

2.1 Materials

Natural rubber latex (dry rubber content 60 phr (per hundred rubbers)) was supplied by Chengyi Rubber Company, Dongguan. $FeCl_3$ and $FeCl_2$ were supplied by Shanxi Wanhua Chemical Company, Potassium hydroxide (KOH), sodium hydroxide (NaOH) and leveling fatty alcohol polyoxyethylene ether (Agent O) were kindly provided by Wanhua Chemical Company and used as stabilizers, Zinc oxide (ZnO) was used as activator, zinc diethyl dithiocarbamate (ZDC) was used as the accelerator, and sulfur (S) was used as the vulcanizing agents. All the reagents were purchased from the Sichuan Haida Rubber Group.

2.2 NR nanocomposite coating based on various carbon nanomaterials

(1) Preparation of the sulfur and additives dispersion solutions

A solution of 6.0 ml NH_3(20.0%) and 20.0 g of casein were added to an aqueous solution under stirring at 50 ℃ to form a stable casein solution (10.0 wt%). KOH (12.5 g) and alkyl polyoxyethylene ether (12.5 g) were added to the aqueous solutions (50.0 ml), stirred at 50℃ to form a mixed solutions (20.0 wt%), respectively.

Then, 50.0 g of sulphur, 20.0 ml of the casein aqueous solution and sand were added to the aqueous solution under stirring for 12.0 h at room temperature. In addition, the sand was removed by a sieve from the mixing solution to form a stable sulphur dispersion solution (50.0 wt%). Next, 20.0 g of ZnO, 3.0 g of the dispersing agent NNO (NF), 40.0 ml of the casein solution and sand were added to the aqueous solution with stirring at room temperature for 12.0 h . In addition, the sand was removed by a sieve from mixing solution to form stable ZnO suspension solution (40.0 wt%). Zinc diethyldithiocarbamate (ZDC) (50.0 g), 1.15 g of NF, 20.0 ml of the casein solution and sand were added to the aqueous solution under stirring for 12.0 h at room temperature. In addition, the sand was removed by a sieve from the above solution and form a stable ZDC dispersion solution (50.0 wt%).

(2) Synthesis of various carbon nanomaterials modified with Fe_3O_4 nanoparticles

First, stable Fe_3O_4 magnetic fluids were prepared by a co-precipitation method, as follows: 3.58 g $FeCl_2 \cdot 4H_2O$ and 6.08 g $FeCl_3 \cdot 6H_2O$ were dissolved in 90.0 ml of distilled water to form a mixing solution. Then, 92.4 ml of solution containing 4.94 g of NaOH was added dropwise into the above solution under stirring. The reaction was sustained at 50.0℃ for 90.0 min. The precipitates of Fe_3O_4 nanoparticles were separated by a magnet. The precipitate was washed with deionized water for several times to remove any excess impurities. GO was prepared by the modified Hummer's method according to reported work [16].

Second, 30.0 ml of Fe_3O_4 magnetic fluid (with 0.2 g Fe_3O_4) was slowly added into the 60.0 ml CNT solution or GO (with 0.25 g CNT or GO) at 40℃ under a nitrogen flow with vigorous stirring. Then, the Fe_3O_4@GO or CNT nanocomposites were separated by an external magnetic field and washed with water for several times to ensure no water among the nanocomposites. The Fe_3O_4@rGO was further prepared by the reducing of the Fe_3O_4@GO solution as described previously [17].

(3) Preparation of the Fe_3O_4@carbon nanomaterials/NR nanocomposite coating

The carbon nanomaterials @Fe_3O_4/NR nanocomposite coating was prepared by a latex compounding process as follows. The Fe_3O_4@carbon nanomaterial dispersion solution, sulfur and other additives in dispersion solutions were successively added to natural rubber latex under mechanical agitating at room temperature to form a uniform and stable compounding latex. And then the compounding latex was spray coated on an iron plate (30.0 mm×10.0 mm×1.0 mm) to form a nanocomposite coating. The nanocomposite coating was further vulcanized at room temperature for 12 h. The experimental formulas are shown in Table1.

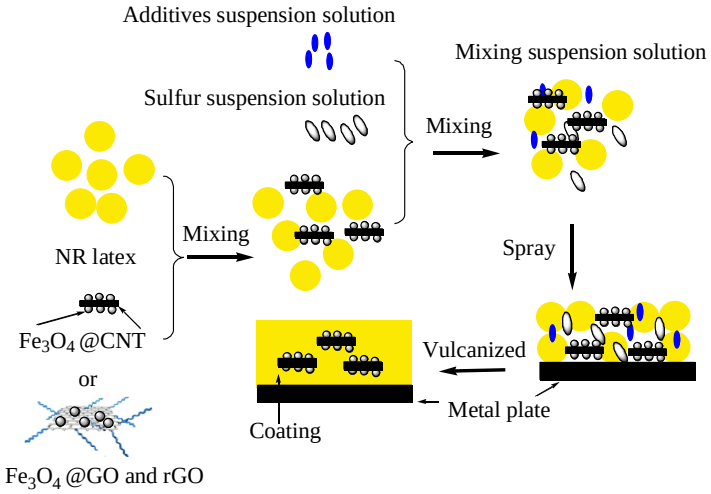

Scheme 1. The preparation process of the NR nanocomposite coating by the latex method.

Table 1. The experimental formula of NR nanocomposite coating by the latex method.

Component	Loading (phr)
NR latex solution (60.0 wt%)	100
Fe_3O_4@carbon nanomaterials(1:1.25)	3.6
KOH solution (20.0 wt%)	0.3
Alkyl polyoxyethylene ether solution (20.0 wt%)	0.3
Sulphur solution (50.0 wt%)	1.2
ZnO solution (40.0 wt%)	0.6
ZDC solution (50.0 wt%)	0.6

2.3 Characterization

The morphology and phase structure of the carbon nanomaterials were investigated by a transmission electron microscope (TEM, JEOL-2100).

The carbon nanomaterials and the NR nanocomposite coating were taken by an inspect scanning electron microscopy (SEM) (SU-4700) instrument (FEI) with an acceleration voltage of 30 kV.

The thicknessof coating was measured by the optical microscopy (105J).

The crystal structure was examined by an XRD diffractometer (Bruker), with a radiation source of Cu Ka at 40 kV and 40 mA (λ = 0.154 nm).

The corrosion evaluation of the coating was performed examined by optical microscope.

2.4 Corrosion properties of the coatings

The corrosion evaluation of the coating was performed via electrochemical analysis. All experiments for corrosion investigations were performed in a NaCl solution (0.1 M). The electrochemical experiments were carried out in a conventional three-electrode cell with a platinum counter electrode and a saturated calomel electrode (SCE) as reference electrode.

The Gill AC Serial no. 947 (ACM instruments) were used to perform electrochemical measurements. Potentiodynamic polarization testing were carried out in a range of ±200 mV at a scan rate of 0.125 mV s^{-1}.

EIS (Electrochemical impedance spectroscopy) were carried out using the 5 mV amplitude AC signals in the frequency range of 100 kHz to 10 mHz. Because of coating thickness variations and the high sensitivity of the EIS technique, scattering of the data is a big challenge for EIS data acquisition. The testings were repeated at least three times to verify the repeatability. To evaluate the parameters of the equivalent electrical circuit, the real (Z') and imaginary (-Z'') components of the impedance spectra were analyzed using the EIS analyzer fitting program.

3. RESULTS AND DISCUSSION

3.1 Preparation of NR nanocomposite coatings based on various carbon nanomaterials

The latex technology was employed to prepare the NR nanocomposite coatings based on carbon nanomaterials and NR latex for applications in corrosion protection. The following two factors should be considered: (1) the sulfur and other additives should be well dispersed and stable in the NR latex to form a uniform and more cross-linked NR coating; (2) the high dispersion and stability of the carbon nanomaterials in the latex solution are required to obtain well-distributed NR nanocomposite coatings. In the present work, sulfur (S), zinc oxide (ZnO), an accelerator ZDC and other additive dispersion solutions with high stabilization were prepared by a facile method.

Here, the carbon nanomaterials modified with Fe_3O_4 nanoparticles were also prepared by a facile method to improve their dispersion in the NR latex. The SEM images of the Fe_3O_4@GO, Fe_3O_4@rGO and Fe_3O_4@CNT nanocomposites are shown in Fig.1. The images show that the synthesized Fe_3O_4@GO and Fe_3O_4@rGO were rigid flakes that formed a film with a rough morphology, and the Fe_3O_4 was uniformly dispersed on the surface of the rGO and GO sheets (in Fig. 1A-B). As shown in Fig. 1C, CNT and Fe_3O_4 were present. The Fe_3O_4@carbon nanomaterial nanocomposites were further characterized by EDS spectra shown in Fig. 1D. The spectra confirmed the presence of C, Fe and O elemental signatures for all the nanocomposites [18]. At the same time, the

spectra also confirmed the similar mass ratios of Fe_3O_4 and carbon in all the nanocomposites, and the loading amount of the carbon nanomaterials in the composites was apprpximately 50.5 wt%. These results further indicated that the Fe_3O_4@GO, Fe_3O_4@rGO and Fe_3O_4@CNT nanocomposites could be prepared on a large scale in the present work.

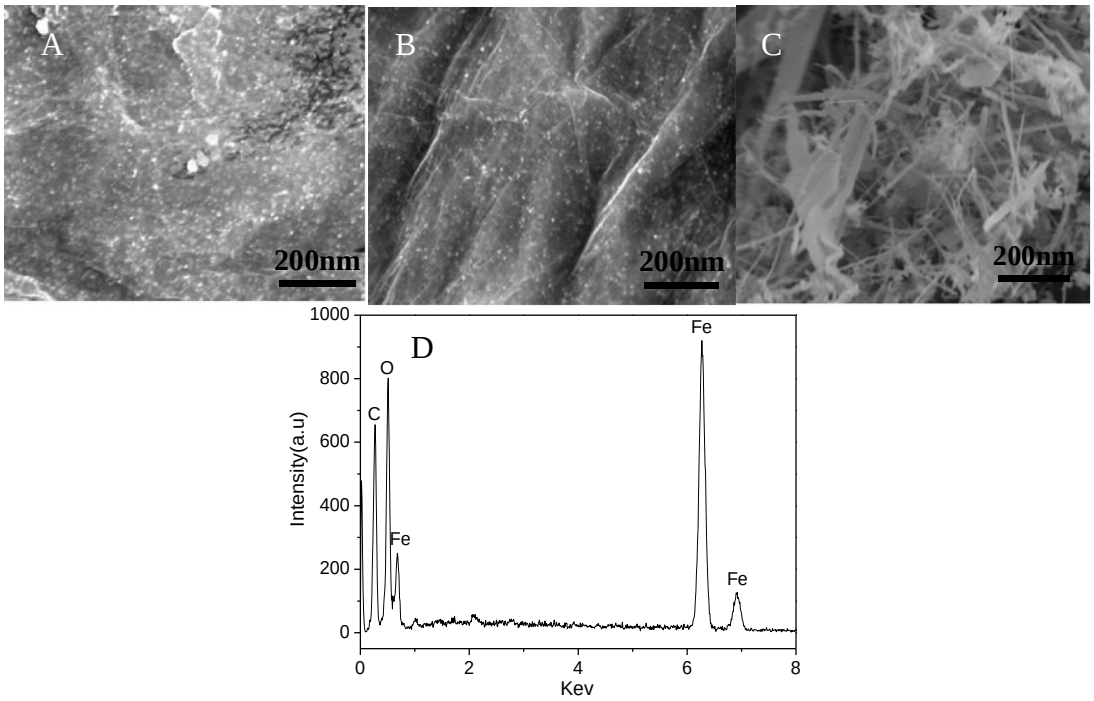

Figure 1. The SEM image of the (A) Fe_3O_4@GO, (B)Fe_3O_4@rGO and (C)Fe_3O_4@CNT nanocomposites. (D) is the EDS of the Fe_3O_4@carbon nanomaterials.

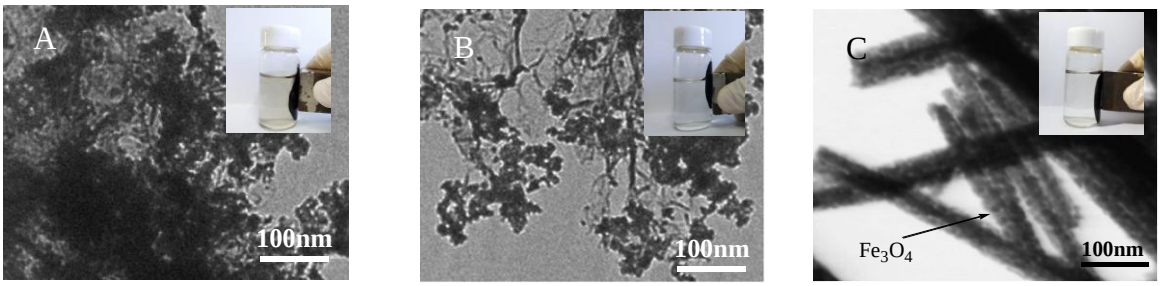

Figure 2. The TEM images of the (A) Fe_3O_4@GO, (B) Fe_3O_4@rGO and (C) Fe_3O_4@CNT nanocomposites.

The structures of the Fe_3O_4@GO, Fe_3O_4@CNT and Fe_3O_4@rGO nanocomposites were further observed by the TEM images as shown in Fig. 2. It can be clearly seen that the Fe_3O_4 nanoparticles were homogeneously distributed on the surface of the rGO, GO and CNT, and the average diameter of the Fe_3O_4 nanoparticles was about 20.0 nm. The Fe_3O_4@GO, Fe_3O_4@CNT and Fe_3O_4@rGO nanocomposites without any surfactants were well dispersed and stable in aqueous solutions.

Additionally, they could be separated completely from the suspension within 5 s by an external magnet, indicating that the Fe_3O_4 was fixed on the surface of the carbon nanomaterials as shown in the inset of Fig. 2 [17]. It is also believed that the Fe_3O_4 nanoparticles anchored on the surface of the carbon nanomaterials act as spacers, which prevents the restacking and aggregation of the carbon nanomaterials, thereby increasing the active surface and dispersion in aqueous solution. Moreover, the nanoparticles were dispersed in the NR latex containing the additives, which was stable without precipitation for at least two months. The nanoparticles acting as spacers were key in the preparation of NR nanocomposite coatings based on carbon nanomaterials with high anticorrosion performance.

The XRD patterns of the Fe_3O_4@GO, Fe_3O_4@CNT and Fe_3O_4@rGO/NR nanocomposite coatings are displayed in Fig. 3. The patterns clearly showed one broad and strong peak at around 18.54°, which was assigned to the amorphous NR matrix for all the samples [19]. Additionally, the other small diffraction peaks at around 30.02°, 35.5°, 43.12°, 53.8°, 62.8° correspond to the (220), (311), (400), (422) and (440) planes of Fe_3O_4, respectively (JCPDS card No. 04-0850), which agreed well with the literature values [17, 19-20]. These results indicated the formation of the Fe_3O_4@GO, Fe_3O_4@CNT and Fe_3O_4@rGO/NR nanocomposite coatings. However, the diffraction peaks assigned to rGO, GO and CNT were difficult to be observed because their diffraction peak positions were covered by the broad and strong peak of NR [12-14].

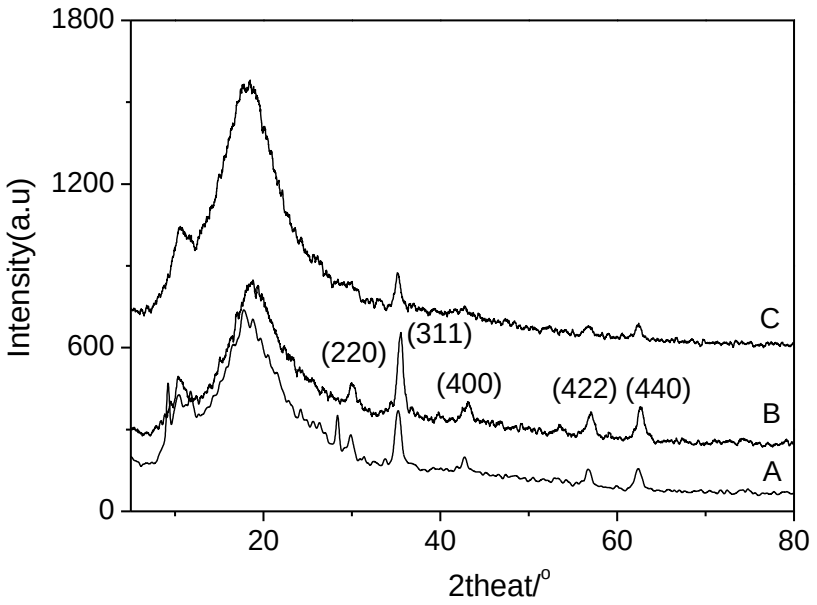

Figure 3. XRD patterns of (A) Fe_3O_4@GO, (B)Fe_3O_4@rGO and (C) Fe_3O_4@CNT/NR nanocomposite coatings.

The nanocomposite coatings coated on an iron plate were also confirmed by the SEM images, shown in Fig. 4. The images clearly showed that the surfaces of the nanocomposite coatings were similar to the neat NR coating, and there were some white spots on the surfaces, which were maybe vulcanization additives [21]. At the same time, some cracks were found in the nanocomposite coatings as shown in Fig. 4A-D. The result was attributable to fact that the air flow in the drying chamber was

weaker and the temperature distribution was uneven during the suspension drying process [14]. Smooth surfaces on the nanocomposite coatings containing various carbon nanomaterials were also observed, and aggregates were rarely found. These results further indicated that the carbon nanomaterials modified with Fe_3O_4 nanoparticles could be well dispersed in a NR coating using the present method.

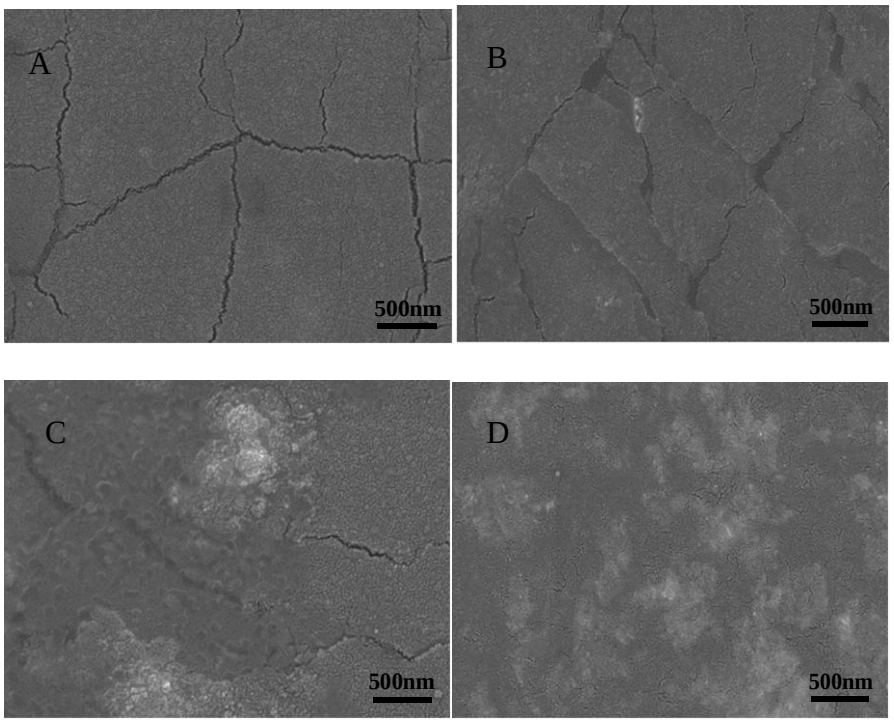

Figure 4. SEM images of (A) NR, (B) Fe_3O_4@GO, (C)Fe_3O_4@rGO and (D)Fe_3O_4@CNT/NR nanocomposite coatings coated on an iron plate.

3.2 Corrosion resistance of the NR nanocomposite coatings based on various carbon nanomaterials

To determine the corrosion resistance of the NR nanocomposite coatings based on various carbon nanomaterials, potentiodynamic polarization tests were performed on uncoated and coated iron plates in 0.1 M NaCl aqueous solution, and the results are presented in Fig. 5. The electrochemical parameters, including the anodic Tafel slope (βa), cathodic Tafel slope (βc), corrosion potential (Ecorr), corrosion current density (Icorr), the corrosion rate (CR, mm/year) and enhanced protection efficiency (EPE, %) were computed and listed in Table 2. It clearly showed that the βa was larger than the βc, indicating that anodic branch of the polarization curve was distorted more severely than the cathodic branch. In addition to this, the βc of coated iron plates was generally larger than that of uncoated iron plates. The result suggested that the uncoated iron plates had faster corrosion rate comparing to coated iron plates. Compared with blank and NR, the corrosion potentials (Ecorr) of the nanocomposite coatings have an obvious positive shift, which revealed that the corrosion tendency of nanocomposite coatings decreased. Among all the samples, the Fe_3O_4@CNT/NR nanocomposite coating had the lowest Icorr of 0.03 $\mu A/cm^2$. In this paper, the corrosion rate (CR, mm/year) and

enhanced protection efficiency (EPE, %) were used to quantitatively estimate the anticorrosion properties of the coatings. The CR was calculated by

$$CR = \frac{kM_m I_{corr}}{n\rho_m} \quad (1)$$

where, k is a constant (3268.5 mol/A), M_m is the molecular weight of the metal (g/mol), n is the number of charge transfer, and ρ_m denotes the metal density (g/cm^3). In addition, the EPE% was evaluated by

$$EPE\% = \frac{I_{corr,1} - I_{corr,i}}{I_{corr,1}} \times 100\% \quad (2)$$

where, $I_{corr,1}$ is the corrosion current density of NR (A/cm^2), and $I_{corr,i}$ is the corrosion current density of sample i (A/cm^2).

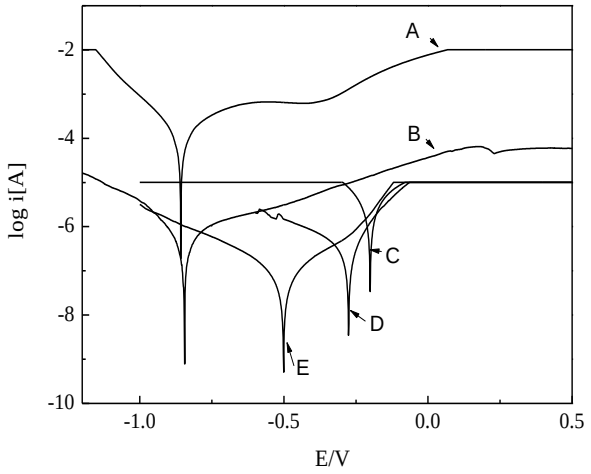

Figure 5. Polarization curves for (A) a blank iron plate, (B) NR, (C) Fe_3O_4@GO, (D)Fe_3O_4@rGO and (E) Fe_3O_4@CNT/NR nanocomposite coatings coated on an iron plate after immersion in a 0.1 M NaCl aqueous solution for 24 h.

The data of the CR and EPE% revealed that the NR nanocomposite coatings had better corrosive protection performance than the NR coating. As all the synthesized carbon materials were nanostructures, it can improve the anticorrosion performance of the NR to embed them in the NR matrix as fillers, and the fillers in the coating matrix usually serves as a barrier. The barrier can increase the coating impermeability by increasing the tortuosity of the diffusion pathway for the molecules in the coating (physical barrier effect). Generally speaking, fillers with higher aspect ratio and larger filler-matrix interfacial area are favorable for raising the tortuosity of the diffusion pathway [1]. The fiber-like Fe_3O_4@CNT should be an outstanding corrosive protection filler for the reasons as follows. Their aspect ratio could be much higher because the lateral dimension of Fe_3O_4@CNT was micrometr scale and the longitudinal dimension was 540.0 nm. In addition, the interfacial area of Fe_3O_4@CNT/NR could be larger because the Fe_3O_4@CNT filler was more likely to unfold in the NR matrix compared with rGO and GO nanosheets.

Table 2. Electrochemical parameters of all specimens in 0.1 M NaCl aqueous solutions

Sample	-βc (V dec^{-1})	βa (V dec^{-1})	I_{corr} (μA/cm^2)	E_{corr} (V)	CR (mm/y)	EPE (%)	Thickness (μm)
Blank iron	0.118	0.167	110.60	-0.862	1.28	--	0
NR	0.113	0.183	10.10	-0.833	1.90×10^{-2}	90.1	10.1
Fe_3O_4@GO/NR	0.134	0.167	1.80	-0.192	1.20×10^{-1}	98.3	9.6
Fe_3O_4@rGO/NR	0.148	0.181	1.40	-0.274	1.60×10^{-2}	98.7	8.9
Fe_3O_4@CNT/NR	0.143	0.154	0.03	-0.505	3.60×10^{-4}	99.9	9.2

EIS was a most important electrochemical technique for the investigation for metal anticorrosion in industrial applications [2]. The Nyquist impedance plots of the uncoated iron plate, the NR coating and the NR nanocomposite coatings based on various carbon nanomaterials coated on iron at 298 K are shown in Fig. 6A-B. All the curves from Fig. 6A-B appear to be similar in shape, but they changed obviously in their size. The Nyquist plots exhibited single depressed semicircles which indicated that the dissolution process was controlled by a charge-transfer reaction [22-23]. At the same time, the EIS spectra were examined by fitting to the equivalent circuit model arranged in such a way Rs in series with the parallel of CPE and Rct shown in Fig. 6C, where Rs was the solution resistance and assigned at the high frequency intercept with the real axis in the Nyquist plots. The CPE (constant phase element) was used to replace a pure capacitor for the deviations in the ideal dielectric behaviors related to the electrode surface in-homogeneity [24]. The impedance (Z) of CPE was given by the expression:

$$Z_{CPE} = Q^{-1}(j\varpi)^{-n} \quad (3)$$

where Q is the CPE constant, ω is the angular frequency, and n is the CPE exponent which gives details about the degree of surface in-homogeneity resulting from the surface roughness, inhibitor adsorption, porous layer formation, etc. [25]. The double layer capacitance could be calculated from:

$$C_{dl} = \left(QR_{ct}^{1-n}\right)^{1/n} \quad (4)$$

From the Rct values, the inhibition efficiency (η_R%) values were obtained from the equation:

$$\eta_R\% = \frac{R_{(coated)} - R_{(uncoated)}}{R_{(coated)}} \times 100\% \quad (5)$$

where Rct (coated) and Rct (uncoated) represented the charge transfer resistance of the coated and uncoated metal, respectively.

Table 3 shows the impedance parameters data for the uncoated and coated iron bipolar plates in 0.1 M NaCl at 298 K. The data showed that the Rct value of the coated iron was obviously higher than that of the uncoated samples. The higher results of Rct was attributed to the effective barrier effect of the NR nanocomposite coating based on the carbon nanomaterials. The lower values of C_{dl} for the coated iron provided further support for the protection of iron by the NR nanocomposite coating. The decrease in C_{dl} was attributed to the better protective layer of coating on the iron surface [26]. The EIS data could be explained by the two thinkable mechanisms. First, carbon nanomaterials reduce the porosity of the coating matrix, prevent the penetration of ions and water into the coating and then

inhibit subsequent electrochemical reactions at the interface of coating/metal, which could lead to the improved the barrier behavior of the NR coating. Second, carbon nanomaterials improved the adherence of the NR coating to the metal surface [3]. The calculated values of η_R% are also given in Table 3. The inhibition efficiency, η_R%, was found to be in the order of CNT>rGO>GO-doped NR nanocomposite coatings and the maximum inhibition efficiency (ca. 99.9%) was obtained for the NR nanocomposite coating based on CNT. These results further indicated that Fe_3O_4@CNT/NR showed the highest barrier behavior, which was in good agreement with the polarization measurements.

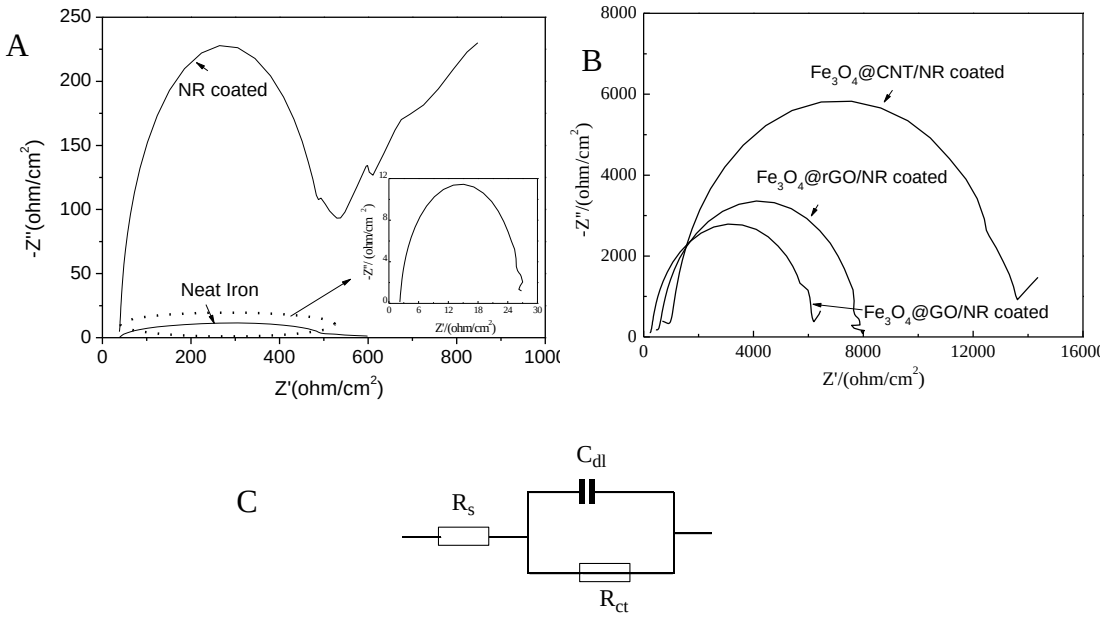

Figure 6. The Nyquist impedance plot for the (A) uncoated and NR-coated iron plates, (B) Fe_3O_4@GO/NR, Fe_3O_4@rGO/NR and Fe_3O_4@CNT/NR-coated iron plates after immersion in a 0.1 M NaCl aqueous solution at 298 K. (C) The proposed equivalent circuit suitable for fitting the EIS results of the coated iron plate.

To evaluate the flexible stability of the NR nanocompoiste coating, a cyclic bending test was implemented, as shown in Fig. 7. Fig. 7A-B show similar polarization curves and the Nyquist impedance plots before and after the ten bending cyclic (ca. 120^o) (in inset of Fig. 7A). And the electrochemical parameters were concluded in Table 4. It could be seen that the Icorr and C_{dl} values for the nanocompsoite coating without a bend treatment sharply increased 40.0% and 25.0% over ten cycles, respectively. While the NR nanocomposite coating showed a good bending performance with only a 10.3% Rct decreased over ten cyclic bending cycles. In addition to this, Fig. 7C-E show the typical optical microscope images of the corroded surfaces of the uncoated and coated iron plates before and after the bending cyclics after 6 days of immersion in a 0.1 M NaCl solution.

Table 3. Impedance parameters and the corresponding inhibition efficiency for uncoated and coated iron bipolar plates in 0.1 M NaCl at 298 K.

Samples	Rs ($\Omega \cdot cm^2$)	Rct($k\Omega \cdot cm^2$)	$C_{dl}(F/cm^2)$	η_R%
iron	2.14	0.024	1.28×10^{-5}	--
NR	13.4	0.498	1.9×10^{-6}	95.2
Fe_3O_4@GO/NR	24.08	5.853	1.2×10^{-6}	99.6
Fe_3O_4@rGO/NR	501.7	7.619	1.6×10^{-6}	99.7
Fe_3O_4@CNT/NR	936.4	12.7	3.6×10^{-7}	99.9

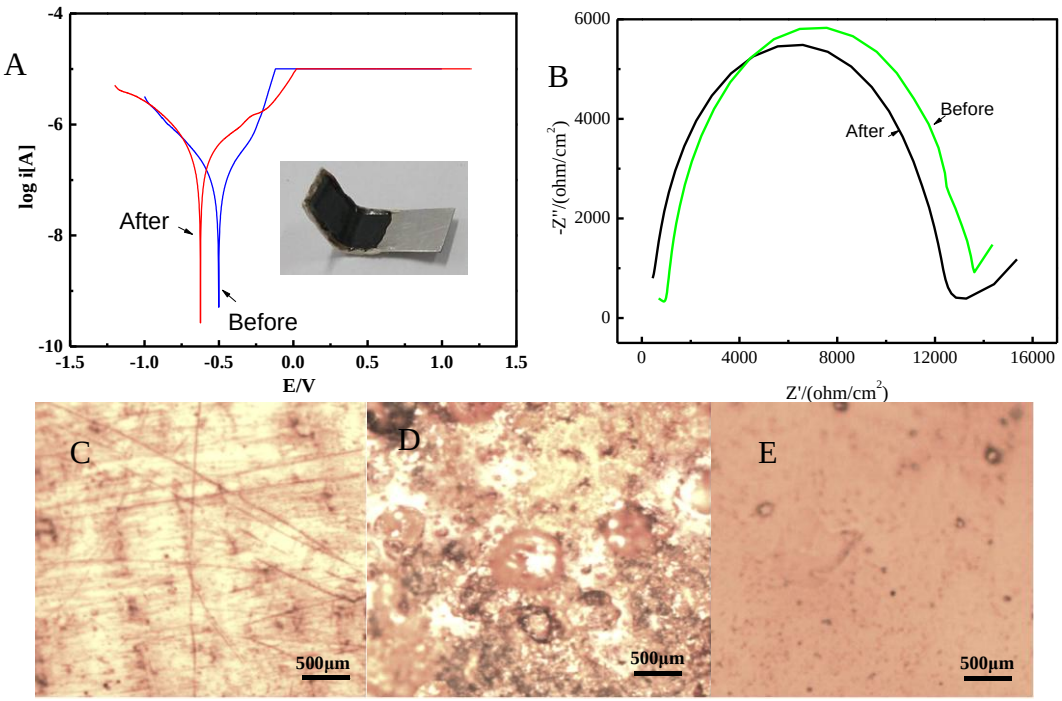

Figure 7. (A) Polarization curves and (B) the Nyquist impedance plots for Fe_3O_4@CNT/NR-coated iron plate before and after bending for 10 cycles in 0.1 M NaCl at 298 K. The optical microscope image of the uncoated iron plate (C) before and (D) after immersion in 0.1 M NaCl at 298 K for 6 days. (E) The optical microscope image of coated iron plate after bending for 10 cycles in 0.1 M NaCl at 298 K for 6 days.

The images clearly showed that no distinct cracks or pitting corrosion were observed for the iron plates coated with the NR nanocomposite coating in comparison with the uncoated specimen (in Fig. 7D). In addition, no changes have been found in the surface of the coated specimen before and after corrosion over ten cycles (Fig. 7C and Fig. 7E, respectively). These results indicated that the NR nanocomposite coating is a good, flexible protective layer for improving the anticorrosive process of metals.

Table 4. Electrochemical parameters and the corresponding inhibition efficiency for the coated iron bipolar plates before and after bending for 10 cycles in 0.1 M NaCl at 298 K.

Bending for 10 cycles	I_{corr}(μA/cm^2)	CR(mm/y)	Rct(kΩcm^2)	C_{dl}(F/cm^2)
before	0.03	3.6×10^{-4}	12.7	3.6×10^{-7}
after	0.05	5.2×10^{-4}	11.6	4.8×10^{-7}

4. CONCLUSIONS

In this study, a NR nanocomposite coating based on different carbon nanomaterials was achieved using a modified latex compounding method, in which the coating could be prepared by spray coating and was vulcanized at room temperature. Furthermore, the corrosion properties studies in 0.1 M NaCl electrolyte by EIS and potentiodynamic polarization tests showed that the carbon nanomaterials modified with Fe_3O_4 nanoparticles in the NR coating considerably reduced the corrosion rate. Interestingly, the Fe_3O_4@CNT/NR nanocomposite coating exhibited a higher corrosion resistance coating than the Fe_3O_4@GO/NR and Fe_3O_4@rGO/NR nanocomposite coatings. Moreover, the NR nanocomposite coating also showed highly flexible anticorrosive properties, and the CR (mm/y) was about 5.2×10^{-4} mm/y after over 10 cyclic bends. This new, flexible anticorrosive coating is expected to be applicable to the corrosion resistance of flexible metal plate and pipes in the future.

ACKNOWLEDGEMENTS
We would like to thank the National Natural Science Foundation of China (11202006), the University's Science and Technology Explorer of Shanxi Province (20140307ZX) and the Shanxi Provincial Natural Science Foundation of China (2014021018-6).

References

1. B. Ramezanzadeh, E. Ghasemi, M. Mahdavian, E. Changizi and M. H. Mohamadzadeh Moghadam, *Carbon*., 93(2015)555.
2. A. Davoodia, S. Honarbakhshb and G. A. Farzi, *Prog. Org. Coat.*, 88(2015)106.
3. A. Ganash,*J. Nanomater.*, 2014 (2014)1.
4. C. H.Chang, T. C. Huang, C. W. Peng, T. C. Yeh and H. I. Lu, *Carbon*., 50(2012)5044.
5. Y. H. Yu, Y. Y. Lin, C. H. Lin, C. C. Chan and Y. C. Huang, *Polym. Chem.*, 5(2014)535.
6. Z. Y. Zhang, W. H. Zhang, D. S. Li, Y. Y. Sun, Z. Wang, C. L. Hou, L. Chen, Y. Cao and Y. Q. Liu, *Int. J. Mol. Sci.*, 16(2015)2239.
7. W. Sun, L. D.Wang, T.T. Wu, Y. Q. Pan and G. C. Liu, *Carbon*., 79(2014)605.
8. B. P. Singh, B. K. Jena, S. Bhattacharjee and L. Besra, *Surf. Coat. Technol.*, 232(2013)475.
9. N. T. Kirkland, T. Schiller, N. Medhekar and N. Birbilis, *Corros. Sci.*, 56(2012)1.
10. K. R. Ratinac, W. Yang, J. J. Gooding, P. Thordarson and F. Braet, Electroanalysis. 23(2011)803.
11. Y. B. Lee, C. H. Lee and D. S. Lim, *Int. J. Hydrogen Energy*., 34(2009)9781.
12. M. A. Deyab, *J. Power Sources*., 268(2014)50.
13. N. Yan, G. Buonocore, M. Lavorgna, S. Kaciulis, S.K. Balijepalli, Y.H. Zhan, H.S. Xia and L.G. Ambrosio, *Compos. Sci. Technol.*, 102(2014)74.

14. F. M. Carolina, F. Galembeck and A. J. G. Zarbin, *Carbon*., 78(2014)469.
15. D. Ponnamma, S. H. Sung, J. S. Hong, K. H. Ahn, K. T. Varughese and S. Thomas, *Eur. Polym. J.*, 53(2014)147.
16. T. T. Liu, G. Z. Zhao, W. H. Zhang, H. J. Chi, C. L. Hou and Y. Y.Sun, *J. Porous. Mat.*, 22(2015)1573.
17. Y. Y. Sun, W. H.Zhang, H. L. Yu, C. L.Hou, D. S. Li, Y. H. Zhang and Y. Q. Liu, *J. Alloys Compd.*, 638(2015)182.
18. Z. Y.Zhang, C. L.Hou, B. S. Shen, Y. Y. Sun, W. H. Zhang,Y. H. Zhang, Y. Q.Liu and L. Gao, *Sci. Adv. Mater.*, 7(2015)1.
19. Y. Y. Sun, X. Zhou, Y. Q. Liu, G. Z. Zhao and Y. Jiang, *Mater. Res. Bull.*, 45(2010)878.
20. Y. Y. Sun, Y. Tian, M. H. He, Q. Zhao, C. Chen, C. S. Hu and Y. Q. Liu, *J. Electron. Mater.*, 41(2012)519.
21. X. L. He, Z. Peng, N. Yu, J.J.Han and C. F. Wu, *Compos. Sci. Technol.*, 68(2008)3027.
22. Y. Y. Sun, W. H. Zhang, D. S. Li, L. Gao, C. L. Hou, Y. H. Zhang and Y. Q. Liu, *Electrochim. Acta.*, 178(2015)823.
23. K. Shimizu, A. Lasia and J. F. Boily, *Langmuir*., 28(2012)7914.
24. T. Tüken, B. Yazıcı and M. Erbil, *Prog. Org. Coat*., 51(2004)152.
25. M. K. Pavithra, T. V. Venkatesha, K. Vathsala and K. O. Nayana, *Corros. Sci.*, 52 (2010) 3811.
26. M. S. Nooshabadi and M. S. Ghandchi, *J. Ind. Eng. Chem.*, 31(2015)231.